

# Analytical Solution for Space-Charge Waves in a Two-Stream Cylindrical Electron Beam

Tarek Mealy, Robert Marosi, Kasra Rouhi, and Filippo Capolino

**Abstract**—We present an analytical method to compute the wavenumbers and electric fields of the space-charge-wave eigenmodes supported by a two-stream electron beam, consisting of a solid inner cylindrical stream and a coaxial outer annular stream, both contained within a cylindrical metallic tunnel. We extend the analytical model developed by Ramo to the case of two streams. The method accounts for the interaction between the two streams with the presence of the beam-tunnel wall; it can be used to model the complex wavenumbers associated with the two-stream instability and the plasma frequency reduction effects in vacuum electronic amplifiers and other vacuum electronic devices.

**Index Terms**—Bifurcation points; Double-stream; Eigenmode solution; Electron beam devices; Exceptional points of degeneracy; Transition points; Two-stream instability.

## I. INTRODUCTION

VACUUM electron devices with high power and broad bandwidth have a competitive edge in various applications, such as electronic countermeasures, satellite communication, plasma diagnostics, and high-resolution radars [1], [2]. Lately, the designers of microwave tubes have faced many difficult design challenges, such as reducing operating voltages and minimizing the weight and dimensions of the devices and their power supplies. In addition, with the high demand for vacuum electronics applications that operate at high frequencies, the dimensions of these devices are being reduced, and at the same time, electron beams with high current density are also required to obtain high output power [3]. There are some technical limitations to increasing both the output power and the operating frequency. The product  $Pf^2$  ( $P$  is the average output power and  $f$  is the frequency of operation), also called the “power density” of the state-of-the-art vacuum electronics is a figure of merit that tends to follow a growing linear trend with time [4]. However, it is not certain how long vacuum electronic devices will continue to follow this trend. A promising engineering solution to continue improving the power density of vacuum electronic devices is to use multiple electron beams [5], [6].

The interaction of multi-stream electron beams has been studied theoretically for years. Many authors have also proposed the multiple beam concept since the 1940s for use

in electron beam devices. As a pioneer in this field, Pierce predicted the gain of a double-stream amplifier having thin concentric electron streams of different velocities that are modulated by input and output cavities. [7]. Then, Swift-Hook analyzed the validity of the theory of the double stream amplification model proposed by Pierce [8]. As an early work on this topic, beam-beam interaction in concentric-beam dual-mode traveling-wave tubes (TWTs) is presented in [9] and then investigated in more detail for various kinds of TWTs in [6]. Chen analyzed the conversion mechanism from the kinetic energy of electron beams to electromagnetic wave energy in the two-stream amplifier and how the efficiency of a two-stream instability amplifier increases with relativistic beam velocities [10]. Wave coupling in multiple beam TWTs to increase the power level of vacuum electronic devices has also been studied in [11]. On the other hand, many works have begun exploring and showing realistic structures for multi-beam generation. In [12], Zavadil proposed a dual-cathode electron gun incorporating an annular hollow beam cathode, concentric and co-planar with a solid beam cathode. Some work has used multiple cathode sources to produce multiple electron beams in low-power microwave sources where two separate power supplies power each cathode at different voltages [13], [14]. Also, some work has been published in the past that uses conventional vacuum electron beam device concepts to generate multiple electron beams [15]–[18]. Multiple electron beam generation with comparable currents and different energies from a single cathode-anode voltage for high power applications has been studied recently in [19], [20]. Another significant motivation for our work has been the analytic theory developed for multi-stream electron beam devices in [21], [22], and the theoretical work involving modal degeneracies in linear beam tubes [23]–[28].

Modern communications’ increasing range and data handling requirements have given rise to a need for microwave tubes with power output and bandwidth capabilities that greatly exceed those of present-day state-of-the-art single-stream electron beam devices. The multiple-beam concept was developed to address this need and was applied to a resonant klystron [29], which was demonstrated to be capable of an order of magnitude higher power output than single-beam devices using the same electron beam. Then the development of multi-beam klystron to provide low operating voltages, high power, low noise, and the possibility of larger operating bandwidth is further studied in many papers such as [5], [30], [31]. Recently, several research papers have focused on electron beam devices that utilize multiple electron streams, namely, multi-beam folded waveguide structures [32]–[35],

Tarek Mealy, Robert Marosi, Kasra Rouhi, and Filippo Capolino are with the Department of Electrical Engineering and Computer Science, University of California, Irvine, Irvine, California, e-mail: tmealy@uci.edu rmarosi@uci.edu kasra.rouhi@uci.edu f.capolino@uci.edu.

This material is based upon work supported by the Air Force Office of Scientific Research award number FA9550-18-1-0355 and by the MURI Award number FA9550-20-1-0409 administered through the University of New Mexico.

two-stream gyrotron TWT amplifiers [36], staggered dual-beam waveguides [37]–[41], dual-beam sine waveguide TWTs [42], [43], and other unique TWT configurations [44]–[48]. The aforementioned devices can employ the advantages of two-stream beams to improve the output power significantly and/or increase the bandwidth for various applications such as telecommunication and high-resolution radar.

The problem of space-charge waves in an electron beam is a topic of interest since such waves are excited and utilized in a variety of electron tubes. These tubes may be used to generate, amplify, and detect signals. Furthermore, such tubes utilizing multi-stream electron beams may either be designed to utilize or avoid strong coupling between electron streams that leads to the two-stream instability under certain conditions. Two-stream instability conditions depend on the velocity differences between electron streams, their respective current densities, operating frequency, and geometry [7]. In particular, Pierce uses an *ad-hoc* separation parameter  $S$  to model how strongly electron streams are coupled when they are close together in a multi-stream beam, which affects the growth rate of space-charge waves under the two-stream instability regime [7]. However, no simple models have yet been developed to analytically determine the growth rate and conditions for two-stream instability as a function of stream geometry, voltage, and current. Ramo studied the propagation of space-charge waves for the case of a single electron beam propagating within a metallic beam tunnel [49]. The theory of Ramo was extended in [50], where they defined the plasma frequency reduction factor and considered the case of an annular electron beam within a cylindrical metallic tunnel. Here, we extend the work of Ramo to the case of two concentric electron streams within a metallic tunnel, which allows us to analytically determine the conditions for two-stream instability and its growth rates without using *ad-hoc* parameters. We consider an electron beam composed of a solid stream inside a hollow coaxial stream as in Fig. 1. Knowledge of the complex propagation constants of space-charge waves supported by the two-stream system may be useful for designing and analyzing two-stream instability amplifiers and two-stream TWTs, which depend strongly on the geometric configuration of the two-stream electron beam.

## II. FORMULATION

### A. Problem Setup

The electron beam is assumed to be made of two concentric streams: stream 1 (the inner stream) is solid with a circular cross section and it exists for  $0 \leq r \leq R_1$ ; stream 2 (the outer stream, coaxial with stream 1) has an annular cross section and it exists for  $R_{i,2} \leq r \leq R_{o,2}$ . The beam tunnel is assumed to be cylindrical with radius  $R_t$  and made of a perfect electric conductor (PEC), as shown in Fig. 1. For convenience, we use a cylindrical coordinate system  $(r, \theta, z)$  in this paper to represent both the beam and the electromagnetic fields.

The two streams are assumed to possess uniform dc charge densities of  $\rho_{0,1}$  and  $\rho_{0,2}$  in both transverse and longitudinal directions. The uniform axial dc magnetic field is assumed to be strong enough to confine each of the two streams such

that all charges travel in the axial direction only (a common simplifying assumption seen in other linear beam tube work such as [7], [49], [51]–[53]) with dc velocities  $u_{0,1}$  and  $u_{0,2}$  for stream 1 and stream 2, respectively. Analogously, the existence of a strong axial dc magnetic field leads also to the assumption that the ac modulation in the velocity of electrons is only in the axial direction. Therefore, the radial and the azimuthal components of electron velocities are assumed to be vanishing [7], [49], [51]–[53]. It is our goal to find the eigenmodes that represent the space-charge waves in this configuration. The propagating space charge wave consists of a modulation in the beam's volumetric charge density and axial velocity, as well as its associated electromagnetic fields, that, in the phasor domain, are all proportional to the wave function  $e^{j(\omega t - kz)}$ . As another simplifying assumption, we only consider modes with azimuthal symmetry; therefore, we assume that  $\partial/\partial\theta = 0$  for all beam and field quantities. However, the presented formalism could be extended to find modes that do not possess azimuthal symmetry. Nevertheless, the case of azimuthal symmetry is the most significant one in practice for TWTs operation. Therefore, the instantaneous total (both dc and ac components) axial velocity and volumetric charge density for each stream are written as

$$\begin{aligned} u_1(r, z, t) &= u_{0,1} + \Re \left( u_{m,1}(r) e^{j\omega t - jkz} \right), \\ u_2(r, z, t) &= u_{0,2} + \Re \left( u_{m,2}(r) e^{j\omega t - jkz} \right), \end{aligned} \quad (1)$$

$$\begin{aligned} \rho_1(r, z, t) &= \rho_{0,1} + \Re \left( \rho_{m,1}(r) e^{j\omega t - jkz} \right), \\ \rho_2(r, z, t) &= \rho_{0,2} + \Re \left( \rho_{m,2}(r) e^{j\omega t - jkz} \right), \end{aligned} \quad (2)$$

where  $u_{m,1}(r)$ ,  $u_{m,2}(r)$ ,  $\rho_{m,1}(r)$  and  $\rho_{m,2}(r)$  are the radial distributions of the stream velocities and charge densities expressed in phasor domain, the subscript '0' denotes the dc component, 'm' denotes ac modulation component, '1' and '2' denote stream 1 and stream 2, respectively. The total radial-dependent volumetric charge density inside the tunnel is expressed as a piecewise function as

$$\rho(r, z, t) = \begin{cases} \rho_1(r, z, t), & 0 \leq r \leq R_1 \\ \rho_2(r, z, t), & R_{i,2} \leq r \leq R_{o,2} \\ 0, & \text{otherwise} \end{cases} \quad (3)$$

We assume that the ac modulation of each electron-beam stream is small compared to the corresponding dc part. Therefore, under this small-signal approximation, the electron beam streams have current densities in the axial direction ( $\mathbf{J}_1 = J_1 \hat{z}$  and  $\mathbf{J}_2 = J_2 \hat{z}$ ) in the form of

$$\begin{aligned} J_1(r, z, t) &= u_1 \rho_1 \approx J_{0,1} + \Re \left( J_{m,1}(r) e^{j\omega t - jkz} \right), \\ J_2(r, z, t) &= u_2 \rho_2 \approx J_{0,2} + \Re \left( J_{m,2}(r) e^{j\omega t - jkz} \right), \end{aligned} \quad (4)$$

where the dc current densities of stream 1 and stream 2 are  $J_{0,1} = \rho_{0,1} u_{0,1}$  and  $J_{0,2} = \rho_{0,2} u_{0,2}$ , and the linearized ac current densities of stream 1 and stream 2 are  $J_{m,1}(r) = \rho_{0,1} u_{m,1}(r) + u_{0,1} \rho_{m,1}(r)$  and  $J_{m,2}(r) = \rho_{0,2} u_{m,2}(r) + u_{0,2} \rho_{m,2}(r)$ , respectively. The total currents for stream 1 and stream 2 are found using integration over each of the transverse cross sections of the stream regions as  $i_1(z, t) = \iint_{A_1} J_1(r, z, t) dA$  and  $i_2(z, t) = \iint_{A_2} J_2(r, z, t) dA$ , where

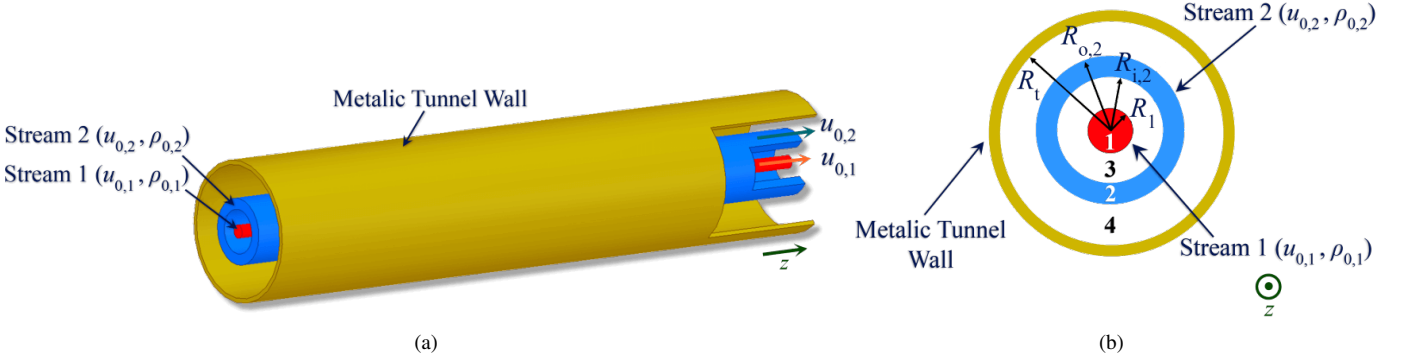


Fig. 1. (a) Double stream electron beam with distinct dc speed and charge density. We show in (b) the transverse cross section for the double stream system, where the area inside of the tunnel is divided into four homogeneous regions. Stream 1 (the inner stream) exists in region 1, whereas stream 2 (the outer stream) exists in region 2, and regions 3 and 4 are vacuum spaces.

$A_1 = \pi R_1^2$  and  $A_2 = \pi (R_{o,2}^2 - R_{i,2}^2)$  are the cross-sectional areas of region 1 and 2, respectively. This integration yields

$$\begin{aligned} i_1(z, t) &= -I_{0,1} + \Re \left( I_{m,1} e^{j\omega t - jkz} \right), \\ i_2(z, t) &= -I_{0,2} + \Re \left( I_{m,2} e^{j\omega t - jkz} \right), \end{aligned} \quad (5)$$

where  $I_{0,1} = A_1 \rho_{0,1} u_{0,1}$  and  $I_{0,2} = A_2 \rho_{0,2} u_{0,2}$  are the dc currents of stream 1 and stream 2, respectively, and  $I_{m,1}$  and  $I_{m,2}$  are the ac currents of stream 1 and stream 2 in phasor domain, respectively.

The electromagnetic fields associated to the two-stream electron beam are represented using the electric scalar potential and magnetic vector potential which are expressed as

$$\phi(r, z, t) = \Re \left( f_\phi(r) e^{j\omega t - jkz} \right), \quad (6)$$

$$\mathbf{A}(r, z, t) = \Re \left( f_A(r) e^{j\omega t - jkz} \right) \hat{\mathbf{z}}, \quad (7)$$

where  $\hat{\mathbf{z}}$  is the unit vector in the  $z$  direction. The chosen magnetic vector potential has only an axial component (in the  $z$  direction) because we assume that only the longitudinal component of current modulation is present (we neglect current directions that are not longitudinal because we assume to have a very high, confining, axial dc magnetic field). We use the International System of Units (SI) in the following analysis, whereas CGS units were used in [49]. The electric and magnetic fields in the structure are expressed in terms of the scalar electric potential and vector magnetic potential as  $\mathbf{E} = -\nabla\phi - d\mathbf{A}/dt$  and  $\mathbf{H} = \nabla \times \mathbf{A}/\mu_0$ . Here, we use the Lorentz gauge  $\nabla \cdot \mathbf{A} = -\mu_0 \epsilon_0 \partial\phi/\partial t$  [54], which leads to the relation  $f_A(r) = \frac{\omega \mu_0 \epsilon_0}{k} f_\phi(r)$ , as shown in Appendix A. Because the tunnel region is not homogeneously filled, we represent the radially-dependent electric scalar potential function  $f_\phi(r)$  in Eq. (6) as

$$f_\phi(r) = \begin{cases} f_{\phi,1}(r), & 0 \leq r \leq R_1 \\ f_{\phi,3}(r), & R_{o,1} \leq r < R_{i,2} \\ f_{\phi,2}(r), & R_{i,2} \leq r < R_{o,2} \\ f_{\phi,4}(r), & R_{o,2} \leq r < R_t \end{cases}. \quad (8)$$

The time-domain electric and magnetic fields (which do not depend on  $\theta$  due to the assumption of azimuthal symmetry) are then given by

$$\begin{aligned} E_r(r, z, t) &= \Re \left( -f'_\phi(r) e^{j\omega t - jkz} \right), \\ E_z(r, z, t) &= \Re \left( \left( j \frac{k^2 - \omega^2 \mu_0 \epsilon_0}{k} \right) f_\phi(r) e^{j\omega t - jkz} \right), \\ H_\theta(r, z, t) &= \Re \left( -\frac{\omega \epsilon_0}{k} f'_\phi(r) e^{j\omega t - jkz} \right), \end{aligned} \quad (9)$$

whereas the rest of time-varying field components are vanishing, i.e.,  $E_\theta = H_r = H_z = 0$ .

### B. Governing Equations

We start by writing Newton's second law, which describes the equations of motion for each stream individually. The basic equations that govern the charges' longitudinal motion are

$$m \frac{du_1}{dt} = -eE_{z,1}, \quad (10)$$

$$m \frac{du_2}{dt} = -eE_{z,2}, \quad (11)$$

where  $E_{z,1}$  and  $E_{z,2}$  are the longitudinal electric fields that stream 1 and stream 2 experience in each of the regions denoted by indices '1' and '2', respectively (See Fig. 1),  $m = 9.109 \times 10^{-31}$  kg is the rest mass of an electron, and  $e = +1.602 \times 10^{-19}$  C is the elementary charge. The longitudinal electric fields  $E_{z,1}$  and  $E_{z,2}$  are determined from Eq. (9) in region 1 and region 2, as we will discuss later. Each electron flow should be continuous and there should be no leakage or accumulation of charges. Therefore, the continuity equation for each stream is written as  $\nabla \cdot \mathbf{J}_1 = -\partial\rho_1/\partial t$  and  $\nabla \cdot \mathbf{J}_2 = -\partial\rho_2/\partial t$  which are simplified as

$$\frac{\partial(\rho_1 u_1)}{\partial z} = -\frac{\partial\rho_1}{\partial t}, \quad (12)$$

$$\frac{\partial(\rho_2 u_2)}{\partial z} = -\frac{\partial\rho_2}{\partial t}. \quad (13)$$

As explained in Appendix A, these charge continuity and force equations lead to the velocity and charge modulations of each stream, expressed in terms of the scalar potential as

$$u_{m,i}(r) = \frac{\eta}{u_{0,i}} \frac{k_0^2 - k^2}{k(k - \beta_{0,i})} f_{\phi,i}(r), \quad (14)$$

$$\rho_{m,i}(r) = -\frac{\eta\rho_{0,i}}{u_{0,i}^2} \frac{k_0^2 - k^2}{(k - \beta_{0,i})^2} f_{\phi,i}(r), \quad (15)$$

where  $i = 1, 2$  refers to stream 1 or 2. Furthermore,  $\beta_{0,i} = \omega/u_{0,i}$  is the electronic phase constant of the  $i$ -th electron stream,  $\eta = e/m = 1.758829 \times 10^{11}$  C/kg is the charge to mass ratio of an electron and  $k_0 = \omega\sqrt{\mu_0\epsilon_0}$ .

Following what was done in [49] for a single-stream electron beam inside a concentric metallic tunnel, the governing equation in each region of our problem is found by substituting the definition  $\mathbf{E} = -\nabla\phi - d\mathbf{A}/dt$  into Gauss' law  $\nabla \cdot \mathbf{E} = \rho/\epsilon_0$ , and by using the Lorentz gauge (see Appendix A), leading to

$$\left(\nabla^2 - \mu_0\epsilon_0 \frac{\partial^2}{\partial t^2}\right)\phi = -\frac{\rho}{\epsilon_0}. \quad (16)$$

The charge density term in Eq. (16) is either  $\rho = 0$ , in the two vacuum regions, or is given by Eq. (15) in the two stream regions. Substituting these values for charge density into Eq. (16), we arrive at the Bessel differential equations for the electric potential in both the vacuum and stream regions, as explained further in Appendices A and B. As a result, in the two stream regions (i.e., regions 1 and 2), the potential solution is expressed in terms of Bessel functions of the first and second kind, and order zero. For the vacuum regions between the electron streams and near the metallic wall (i.e., regions 3 and 4), the potential solution is written in terms of modified Bessel functions of the first and second kind, of order zero. An alternative formulation is based on taking the electric field expressions in Eq. (9) and the charge density expression in Eq. (15) into Gauss' law  $\nabla \cdot \mathbf{E} = \rho/\epsilon_0$ , and the Bessel equations are determined by expressing everything in terms of  $f_\phi(r)$ .

### C. Boundary Conditions

Aside from the fact that the potential function  $f_\phi(r)$  is finite at  $r = 0$ , following what was done in [49], we also enforce that the potential function  $f_\phi(r)$  and its derivative are continuous across the boundaries between the concentric regions illustrated in Fig. 1 as

$$\begin{aligned} f_{\phi,1}(R_1) &= f_{\phi,3}(R_1), & f'_{\phi,1}(R_1) &= f'_{\phi,3}(R_1), \\ f_{\phi,3}(R_{i,2}) &= f_{\phi,2}(R_{i,2}), & f'_{\phi,3}(R_{i,2}) &= f'_{\phi,2}(R_{i,2}), \\ f_{\phi,2}(R_{o,2}) &= f_{\phi,4}(R_{o,2}), & f'_{\phi,2}(R_{o,2}) &= f'_{\phi,4}(R_{o,2}). \end{aligned} \quad (17)$$

Due to the assumption that a tunnel is made of PEC, we also enforce that the potential function vanishes at the tunnel wall

$$f_{\phi,4}(R_t) = 0. \quad (18)$$

In the following section, we describe the solution of the potential functions in each region. Then, we enforce the aforementioned boundary conditions to find a linear system whose solution provides the eigenmodes of charge waves in this system.

## III. MODAL DISPERSION EQUATION

The general solutions of the scalar electric potential as a function of radius in each region shown in Fig. 1 are found based on the derivation in Appendices A and B. We write the radially-dependent scalar potential function in Eq. (8) as

$$f_{\phi,1}(r) = c_1 J_0(T_1 r), \quad (19)$$

$$f_{\phi,3}(r) = c_2 K_0(\tau r) + c_3 I_0(\tau r), \quad (20)$$

$$f_{\phi,2}(r) = c_4 J_0(T_2 r) + c_5 Y_0(T_2 r), \quad (21)$$

$$f_{\phi,4}(r) = c_6 K_0(\tau r) + c_7 I_0(\tau r), \quad (22)$$

where  $c_n$  ( $n = 1, \dots, 7$ ) are arbitrary constants that are determined by imposing the boundary conditions in Sec. II-C. The parameters  $T_1$  and  $T_2$  in the arguments of the above Bessel functions are related to regions 1 and 2, i.e., in the electron streams, and the parameter  $\tau$  is related to the vacuum regions outside of the electron streams (regions 3 and 4), defined as

$$T_1^2 = \tau^2 \left( \frac{(\beta_{p,1})^2 - (k - \beta_{0,1})^2}{(k - \beta_{0,1})^2} \right), \quad (23)$$

$$T_2^2 = \tau^2 \left( \frac{(\beta_{p,2})^2 - (k - \beta_{0,2})^2}{(k - \beta_{0,2})^2} \right), \quad (24)$$

$$\tau^2 = (k^2 - k_0^2). \quad (25)$$

In these equations,  $\beta_{p,1} = \omega_{p,1}/u_{0,1}$  and  $\beta_{p,2} = \omega_{p,2}/u_{0,2}$  are the plasma phase constants related to stream 1 and stream 2, respectively, related to the two plasma frequencies  $\omega_{p,1} = \sqrt{\eta\rho_{0,1}/\epsilon_0}$  and  $\omega_{p,2} = \sqrt{\eta\rho_{0,2}/\epsilon_0}$ . Note that we did not consider the Bessel's function of the second kind (Neumann's function)  $Y_0(T_1 r)$  in  $f_{\phi,1}(r)$  because the scalar potential should be finite at  $r = 0$ , and  $Y_0(T_1 r)$  has a singularity at  $r = 0$ . When the six boundary conditions in Eq. (17) are enforced, together with the PEC condition at the tunnel wall in Eq. (18), the resulting set of seven equations are cast in matrix form as  $\underline{\mathbf{M}}\mathbf{c} = \mathbf{0}$ , where  $\mathbf{c} = [c_1, c_2, c_3, c_4, c_5, c_6, c_7]^T$  ( $T$  denotes the transpose operation) and the matrix  $\underline{\mathbf{M}}$  is defined as

$$\underline{\mathbf{M}} = \begin{bmatrix} J_0(T_1 R_1) & -K_0(\tau R_1) & -I_0(\tau R_1) & 0 & 0 & 0 & 0 & 0 \\ T_1 J_0'(T_1 R_1) & -\tau K_0'(\tau R_1) & -\tau I_0'(\tau R_1) & 0 & 0 & 0 & 0 & 0 \\ 0 & K_0(\tau R_{i,2}) & I_0(\tau R_{i,2}) & -J_0(T_2 R_{i,2}) & -Y_0(T_2 R_{i,2}) & 0 & 0 & 0 \\ 0 & \tau K_0'(\tau R_{i,2}) & \tau I_0'(\tau R_{i,2}) & -T_2 J_0'(T_2 R_{i,2}) & -T_2 Y_0'(T_2 R_{i,2}) & 0 & 0 & 0 \\ 0 & 0 & 0 & J_0(T_2 R_{o,2}) & Y_0(T_2 R_{o,2}) & -K_0(\tau R_{o,2}) & -I_0(\tau R_{o,2}) & 0 \\ 0 & 0 & 0 & T_2 J_0'(T_2 R_{o,2}) & T_2 Y_0'(T_2 R_{o,2}) & -\tau K_0'(\tau R_{o,2}) & -\tau I_0'(\tau R_{o,2}) & 0 \\ 0 & 0 & 0 & 0 & 0 & K_0(\tau R_t) & I_0(\tau R_t) & 0 \end{bmatrix}. \quad (26)$$

A solution exists when one finds  $k$  such that  $\det(\underline{\mathbf{M}}) = 0$ . Here, we look for complex  $k$  solutions, though they may also be purely real. The matrix  $\underline{\mathbf{M}}$  may become ill-conditioned (i.e., the condition number of the matrix becomes large [55]) when using an imaginary part of the wavenumber  $k$  that makes the Bessel functions extremely large or small in value. This also occurs when  $k$  is nearly equal to  $\beta_{0,1}$  or  $\beta_{0,2}$ , which are the poles of  $T_1$  and  $T_2$ , respectively. To overcome this issue, we follow the same procedure as in [49], i.e., we reduce the number of equations describing the boundary conditions until we obtain only one characteristic equation,  $C_e$ , that is described in terms of the space charge wavenumber  $k$  of the system. Numerical solutions for  $k$  which make  $|C_e| = 0$  are eigenmode solutions of the two-stream system.

#### IV. ILLUSTRATIVE EXAMPLES

As an illustrative example, we consider an electron beam consisting of two streams that have equivalent kinetic dc voltages of  $V_{0,1} = 7$  kV and  $V_{0,2} = 6$  kV, corresponding to average electron speeds of  $u_{0,1} = 0.164c$  and  $u_{0,2} = 0.152c$ , respectively, from the relativistic relation  $V_0 = (\sqrt{1 - (u_0/c)^2} - 1) c^2/\eta$ . Stream 1 is a solid cylinder with a circular cross-section and has an outer radius  $R_1 = 0.1$  mm. Stream 2 is annular in cross section, with inner and outer radii of  $R_{i,2} = 1$  mm and  $R_{o,2} = 1.1$  mm, respectively. The metallic tunnel is made of a PEC and has an inner radius of  $R_t = 2$  mm, as illustrated in Fig. 1. The dc currents of stream 1 and stream 2 are  $I_{0,1} = A_1 \rho_{0,1} u_{0,1} = 50$  mA and  $I_{0,2} = A_2 \rho_{0,2} u_{0,2} = 50$  mA, respectively, corresponding to dc volume charge densities of  $\rho_{0,1} = 0.0325$  C/m<sup>3</sup> and  $\rho_{0,2} = 0.00166$  C/m<sup>3</sup> for streams 1 and 2, respectively.

We show in Fig. 2(a) the magnitude of the characteristic equation,  $C_e$ , defined in Appendix C, in log scale when the real and imaginary parts of  $k$  are swept at a fixed frequency of  $f = 5$  GHz. The roots of the characteristic equation correspond to locations in Fig. 2(a) where  $C_e$  tends to zero (shown by the dark blue regions). We label the four modes in Fig. 2(a) that correspond to the dominant modes of the system. We also verify that, for the four  $k$  solutions, the scalar potential function  $f_\phi(r)$  is continuous at the radii, where we have the boundaries between the electron stream and vacuum regions. The points in the complex  $k$  plane of Fig. 2(a) where  $C_e$  is not vanishing (i.e., everywhere, except for the labeled four solutions) correspond to scalar potential functions  $f_\phi(r)$  that have discontinuities at the radii corresponding to the boundaries between regions. Thus, these points are not valid solutions. The radial profiles of the scalar electric potential

for the four dominant modes labeled in Fig. 2(a) are shown in Fig. 2(b), Fig. 2(c), Fig. 2(d) and Fig. 2(e).

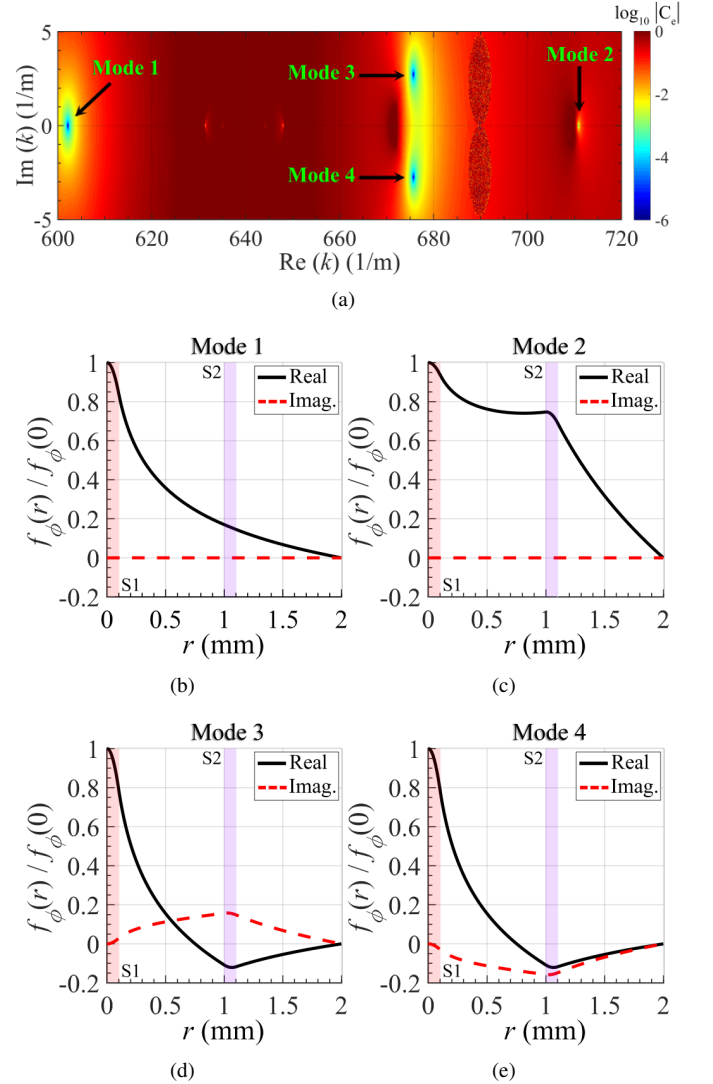


Fig. 2. (a) Values of  $C_e$  versus complex wavenumber  $k$ , evaluated at  $f = 5$  GHz. The labeled points where  $C_e \rightarrow 0$  represent the wavenumber solutions of the system. (b)-(e) Normalized potential profiles corresponding to modes labeled in (a). The radial distribution of the potential function confirms the validity of the solution because one can observe the continuity of the potential function and its derivative at the boundaries between the electron streams and vacuum and its vanishing at the tunnel wall at  $R_t = 2$  mm. The shaded regions in (b)-(e) represent the radial locations of stream 1 and stream 2.

In Fig. 3, we show the four modes of the two-stream system when the dc current of stream 2 is swept, while the dc current of stream 1 is held constant at  $I_{0,1} = 50$  mA.

The frequency is fixed at  $f = 5$  GHz, and the equivalent kinetic stream voltages are held constant at  $V_{0,1} = 7$  kV and  $V_{0,2} = 6$  kV. Also, the study can be used to verify the validity of the mode-finding method that we use. When the dc current of stream 2 approaches zero, this is equivalent to a case where stream 1 only exists in the tunnel. Therefore, when  $I_{0,2} \rightarrow 0$  one sees only two solutions that coincide with the two conventional plasma modes that have wavenumbers described as  $k = \beta_{0,1} \pm \beta_{q,1}$ , where  $\beta_{q,1} = R_{sc}\omega_{p,1}/u_{0,1}$ , and  $R_{sc}$  is the plasma frequency reduction factor, calculated using the method shown in [50]. Figure 3 shows that there exist two transition points (bifurcations) close to  $I_{0,2} = 2$  mA and  $I_{0,2} = 62.2$  mA, between which, exponentially growing space-charge waves occur due to the two-stream instability effect, which happens when there is a sufficient velocity difference between electron streams and sufficient stream currents, as predicted in [7], [56] using an abstract theoretical model. The bifurcation points in Fig. 3 are exceptional points of degeneracy (EPDs) [25], [27], [57], which are conditions where two or more eigenmodes coalesce in their wavenumbers and eigenvectors. In Appendix D we show the effect of swapping the two stream velocities on the resulting space charge wavenumbers. We find that the dispersion diagram does not change significantly compared to the case studied in this section.

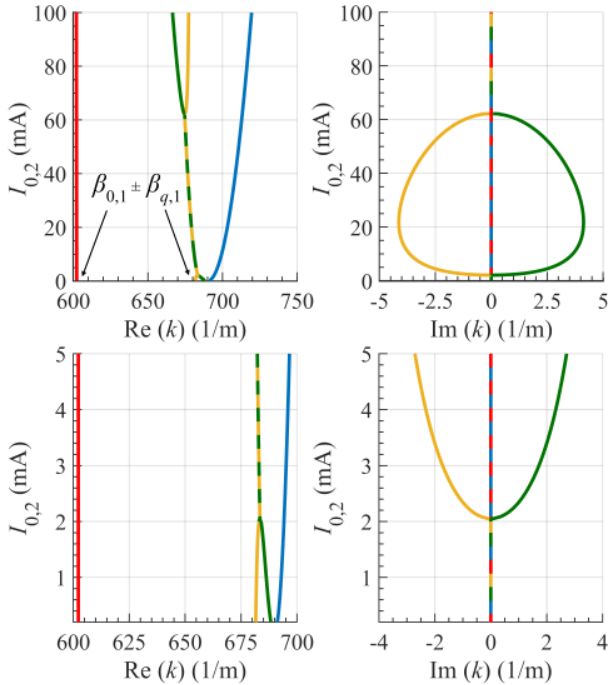


Fig. 3. Top: Modal dispersion diagram of the four complex-valued space-charge wavenumbers as a function of stream 2 dc current. Bottom: magnified version around the EPD for lower values of the current  $I_{0,2}$ .

To understand the conditions resulting in the beam instability, we have swept both dc currents of stream 1 and stream 2 at a fixed frequency of  $f = 5$  GHz and fixed equivalent kinetic stream voltages of  $V_{0,1} = 7$  kV and  $V_{0,2} = 6$  kV, and we monitored the imaginary part of the wavenumber of the growing mode to observe what conditions result in

instability. We show in Fig. 4 the absolute value of the imaginary part of the wavenumber for the modes that exhibit instability, which is depicted by the color area between the two dashed white curves. We see that  $\text{Im}(k) = 0$  outside of the dashed white curves (i.e., shown by dark blue). The dashed white boundary between the region where the wavenumber has  $\text{Im}(k) = 0$  and the colored region where  $\text{Im}(k) \neq 0$  is a curve showing the transition points, or EPDs, where the two-stream instability begins to occur as labeled in Fig. 4. Fixing  $I_{0,1} = 50$  mA and sweeping  $I_{0,2}$  in Fig. 4, results in a curve very similar to that shown in Fig. 3 depicting the imaginary part of the wavenumber showing the two bifurcation points at  $I_{0,2} = 2$  mA and  $I_{0,2} = 62.2$  mA. Figure 4 indicates that charge wave amplification occurs only for certain combinations of stream 1 and stream 2 currents for a given set of frequency and beam parameters.

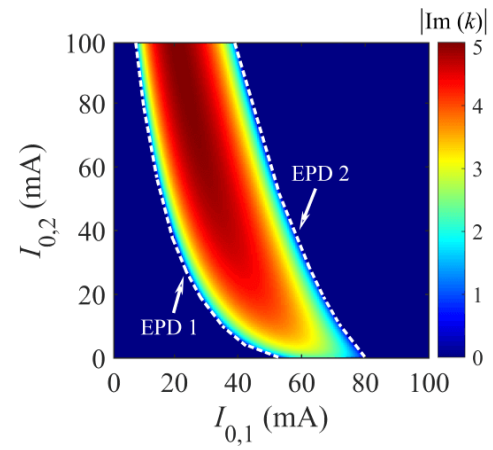


Fig. 4. Contour showing transition boundaries in dashed white curves (labeled EPD 1 and EPD 2), where the imaginary part of the space-charge wavenumber vanishes. Between these boundaries,  $\text{Im}(k) \neq 0$  and two-stream instability occurs for different combinations of stream dc currents.

We repeat the previous study when both dc voltages of stream 1 and stream 2 are swept at a fixed frequency of  $f = 5$  GHz and the beam currents are held constant at  $I_{0,1} = 50$  mA and  $I_{0,2} = 50$  mA. We show in Fig. 5 the absolute value of the imaginary part of the wavenumber for the mode that exhibits a growing instability. Note that instability occurs when either stream 1 has a higher dc voltage than stream 2 or vice versa. Like in the previous figure, the dashed white lines represent the boundary between the stability and instability regions. For the studied range of stream 1 and stream 2 dc voltages in Fig. 5, one finds that instability occurs when the difference between the equivalent kinetic dc voltages of the two streams is approximately  $1 \text{ kV} \lesssim |V_{0,1} - V_{0,2}| \lesssim 1.5 \text{ kV}$ .

We show the modal wavenumber-frequency dispersion relation for the two-stream system in Fig. 6 when the operating frequency is swept while the two beam currents are held constant at  $I_{0,1} = 50$  mA and  $I_{0,2} = 50$  mA and the equivalent stream voltages are held constant at  $V_{0,1} = 7$  kV and  $V_{0,2} = 6$  kV (as in the first and second examples above). The figure shows that the amplification resulting from the two-stream instability occurs from dc up to a threshold frequency, which is 15 GHz in this case (note that the cutoff frequency

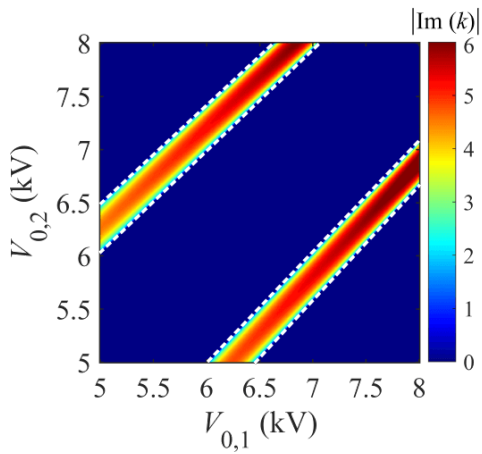


Fig. 5. Contour showing the transition boundaries where the imaginary part of the space-charge wavenumber vanishes. The colored region between dashed white lines represents the region where  $\text{Im}(k) \neq 0$  and two-stream instability occurs for different combinations of stream dc voltages. The dashed white lines indicate the transition boundaries that separate the regions where  $\text{Im}(k) = 0$  from regions where  $\text{Im}(k) \neq 0$  that lead to stream instability.

of the lowest mode ( $\text{TE}_{11}$ ) in a metallic circular waveguide of radius  $R_t = 2$  mm is approximately 44 GHz). For the case of a two-stream instability amplifier, which has been experimentally investigated in works such as [13], [16], it may be potentially beneficial to have a growing instability up to a threshold frequency that is below the lowest cutoff frequency of a circular waveguide, since the device will be less susceptible to regenerative oscillations or backward-wave oscillations that would otherwise exist on a slow-wave structure in a conventional TWT amplifier, as explained in [10]. However, in [58], it was stated that backward-wave oscillations may still be an issue if long slow-wave structures are used to extract amplified waves from a two-stream amplifier.

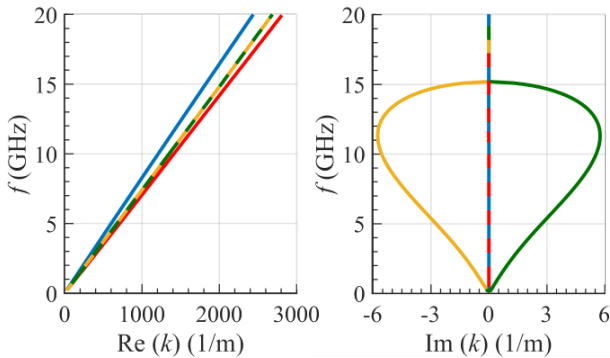


Fig. 6. Modal dispersion showing the four complex space-charge wavenumbers as a function of frequency.

Next, observing the modal dispersion of the wavenumbers as the distance between the two streams varies, Fig. 7, gives us a better understanding of how the two streams are coupled. The coupling is controlled in this example by sweeping the inner radius  $R_{i,2}$  of stream 2 while keeping its width,  $R_{o,2} - R_{i,2} = 0.1$  mm, constant. We also keep the radius of stream 1 constant at  $R_1 = 0.1$  mm. Therefore, what varies is the distance between the two streams,  $R_{i,2} - R_1$ . In Fig. 7 we show the four complex wavenumbers of the two charge-wave

eigenmodes versus  $R_{i,2}$ . The operating frequency is still kept at  $f = 5$  GHz, the currents of the streams are  $I_{0,1} = 50$  mA and  $I_{0,2} = 50$  mA, and the equivalent kinetic voltages of the streams are still kept at  $V_{0,1} = 7$  kV and  $V_{0,2} = 6$  kV. Note that the radius  $R_{i,2} = 1$  mm was considered in all the previous examples, and that for the given values of  $I_{0,1}$ ,  $I_{0,2}$ ,  $V_{0,1}$ , and  $V_{0,2}$  considered here, the two-stream electron beam exhibits instability, as was shown in Fig. 3. The plots in Fig. 7 reveal that when the distance between the two beams  $R_{i,2} - R_1$  gets smaller, the  $\text{Im}(k)$  of the unstable eigenmode gets larger. Conversely, when the distance between the streams gets larger,  $\text{Im}(k)$  gets smaller. Furthermore, for all values of the distance  $R_{i,2} - R_1$ , there are always two eigenmodes with purely real  $k$ , represented by the red and blue curves, and the difference between their  $k$  values remains more or less constant for all considered distances  $R_{i,2} - R_1$ .

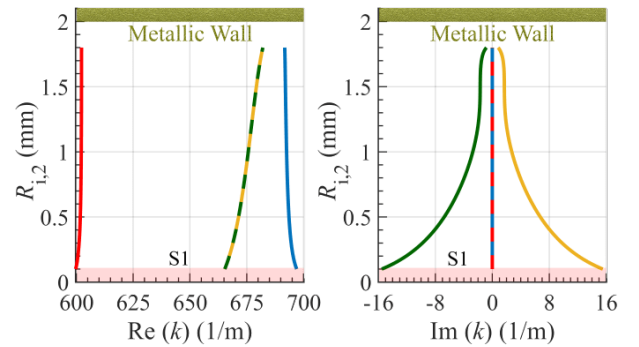


Fig. 7. The real and imaginary parts of the wavenumber  $k$  of the four space-charge modes as a function of the inner radius of stream 2. The shaded region S1 at the bottom indicates the region where stream 1 exists.

## V. CONCLUSION

We have provided an analytical method to determine the wavenumbers and associated electric fields of space-charge waves supported by an electron beam made of two coaxial streams. Our analytical model has determined the two-stream instability regions and the bifurcation points in the wavenumber-dispersion diagrams for a coaxial two-stream system. Specific combinations of dc current and dc equivalent kinetic voltages cause instability. Additionally, this instability growth rate is enhanced when the two streams are closer together. The findings of this work can also be used to build an equivalent transmission line model that describes the two streams' interaction, in analogy to what was done earlier in the analysis of single-stream TWTs and BWOs [24], [27], [51], [52], [59]; such a model can be used in the analysis of amplifiers based on two interacting streams, as proposed in [21], [22]. The method presented in this paper is useful for modeling electron beam systems consisting of two coaxial streams, such as those generated by multi-stream electron guns described in [14], [19], [20].

## APPENDIX A

GENERAL SOLUTION OF THE SCALAR ELECTRIC  
POTENTIAL FUNCTION IN A REGION WITH MOVING  
ELECTRONS (STREAM REGION)

We provide the basic steps to find the general solution that satisfies the differential equation governing the electron beam and the electromagnetic fields. For a given region containing a single electron stream (i.e., either region 1 or 2 in Fig. 1(b)), the electrons in that stream are assumed to be traveling only in the axial direction with uniform dc velocity  $u_0$  and uniform dc charge density  $\rho_0$  (e.g., region 1 in Fig. 1(b) has  $u_0 = u_{0,1}$  and  $\rho_0 = \rho_{0,1}$ ). We assume that the electron beam and the electromagnetic dynamics follow a time-harmonic wave function  $e^{j\omega t - jkz}$  that involves modulation in the charges' axial speed and charge density, which in cylindrical coordinates are written as

$$u(r, z, t) = u_0 + \Re(u_m(r)e^{j\omega t - jkz}), \quad (27)$$

$$\rho(r, z, t) = \rho_0 + \Re(\rho_m(r)e^{j\omega t - jkz}), \quad (28)$$

$$\phi(r, z, t) = \Re(f_\phi(r)e^{j\omega t - jkz}), \quad (29)$$

$$\mathbf{A}(r, z, t) = \Re(f_A(r)e^{j\omega t - jkz}) \hat{\mathbf{z}}. \quad (30)$$

Because of the strong external axial magnetic field that confines the beam, we have assumed that the beam modulation occurs only along the axial direction. Starting from the divergence relation of the magnetic vector potential  $\nabla \cdot \mathbf{A} = -\mu_0 \varepsilon_0 \partial \phi / \partial t$ , one finds that

$$f_A(r) = \frac{\omega \mu_0 \varepsilon_0}{k} f_\phi(r). \quad (31)$$

The axial electric field component is found using the relation  $\mathbf{E} = -\nabla \phi - \partial \mathbf{A} / \partial t$ , which yields

$$E_z(r, z, t) = -\frac{\partial \phi}{\partial z} - \frac{\partial (\mathbf{A} \cdot \hat{\mathbf{z}})}{\partial t} = \Re((jk f_\phi(r) - j\omega f_A(r)) e^{j\omega t - jkz}). \quad (32)$$

We use the relation in Eq. (31) to simplify Eq. (32) as

$$E_z(r, z, t) = \Re\left(\left(j \frac{k^2 - \omega^2 \mu_0 \varepsilon_0}{k}\right) f_\phi(r) e^{j\omega t - jkz}\right). \quad (33)$$

Newton's second law that describes the equation of motion for electrons (for a strongly confined beam of electrons, i.e., with no radial or azimuthal motion) is written as  $m du/dt = -eE_z$ . First, we express the total derivative of the velocity of the electrons in the phasor domain as

$$\frac{du}{dt} = \frac{\partial u}{\partial t} + u_0 \frac{\partial u}{\partial z} = \Re((j\omega - jku_0) u_m(r) e^{j\omega t - jkz}). \quad (34)$$

When this is inserted into Newton's second law applied to the electrons, we find the relation between the velocity and electric potential functions as

$$u_m(r) = \frac{\eta}{u_0} \frac{k_0^2 - k^2}{k(k - \beta_0)} f_\phi(r), \quad (35)$$

where  $k_0 = \omega \sqrt{\mu_0 \varepsilon_0}$  is the free space wavenumber and  $\beta_0 = \omega / u_0$  for the stream-containing region of interest. Moreover, we consider the continuity equation or conservation of charge,

$$\frac{\partial(\rho u)}{\partial z} = -\frac{\partial \rho}{\partial t}, \quad (36)$$

which is simplified to

$$\rho_m(r) = \frac{k \rho_0}{u_0 (\beta_0 - k)} u_m(r). \quad (37)$$

By substituting Eq. (35) into Eq. (37), the latter equation yields the relation between the charge density and the potential function as

$$\rho_m(r) = -\frac{\eta \rho_0}{u_0^2} \frac{k_0^2 - k^2}{(k - \beta_0)^2} f_\phi(r). \quad (38)$$

The final equation that is used to find the potential function is obtained from Gauss' law,  $\nabla \cdot \mathbf{E} = \rho / \varepsilon_0$ , where  $\mathbf{E} = -\nabla \phi - d\mathbf{A}/dt$ , leading to

$$\nabla^2 \phi - \frac{\partial}{\partial t} (\nabla \cdot \mathbf{A}) = -\frac{\rho}{\varepsilon_0}. \quad (39)$$

Then, using the Lorentz gauge  $\nabla \cdot \mathbf{A} = -\mu_0 \varepsilon_0 \partial \phi / \partial t$ , we obtain the inhomogeneous wave equation that governs the scalar electric potential  $(\nabla^2 - \mu_0 \varepsilon_0 \frac{d^2}{dt^2}) \phi = -\rho / \varepsilon_0$ , where the charge density is cast in terms of the scalar potential function  $f_\phi(r)$  using Eq. (38). Due to the azimuthal symmetry of our system in cylindrical coordinates, we have  $\nabla^2 \phi = \frac{1}{r} \frac{\partial}{\partial r} \left( r \frac{\partial \phi}{\partial r} \right) + \frac{\partial^2 \phi}{\partial z^2}$ . After taking the time and  $z$  derivatives, the final equation to be solved is

$$\frac{d^2 f_\phi(r)}{dr^2} + \frac{1}{r} \frac{df_\phi(r)}{dr} + T^2 f_\phi(r) = 0, \quad (40)$$

where

$$T^2 = (k^2 - k_0^2) \left( \frac{\beta_p^2 - (k - \beta_0)^2}{(k - \beta_0)^2} \right). \quad (41)$$

Here,  $\beta_p = \omega_p / u_0$ , and  $\omega_p = \sqrt{\eta \rho_0 / \varepsilon_0}$  is the plasma frequency of the electron stream in the region considered (either stream 1 or stream 2). The general solution of the differential equation in Eq. (40) is written in terms of Bessel's functions as

$$f_\phi(r) = a_1 J_0(Tr) + a_2 Y_0(Tr), \quad (42)$$

where  $a_1$  and  $a_2$  are arbitrary constants,  $J_0$  is the Bessel function of the first kind and order zero, and  $Y_0$  is the Bessel function of the second kind (Neumann's function) of order zero.

One may also find the general solution in terms of modified Bessel's functions, as follows. By transforming the differential equation in Eq. (40) using  $\kappa = jr$ , as was done in [60], we find



$$\frac{d^2 g(\kappa)}{d\kappa^2} + \frac{1}{\kappa} \frac{dg(\kappa)}{d\kappa} - T^2 g(\kappa) = 0, \quad (43)$$

which has a general solution  $g(\kappa) = d_1 I_0(T\kappa) + d_2 K_0(T\kappa)$ . Thus, one may rewrite the general solution of Eq. (42) in terms of modified Bessel functions as  $f_\phi(r) = d_1 I_0(jTr) + d_2 K_0(jTr)$ .

#### APPENDIX B

##### GENERAL SOLUTION OF THE SCALAR ELECTRIC POTENTIAL FUNCTION IN AN EMPTY REGION (VACUUM)

We consider the case where the studied region is empty, i.e., it does not contain charges. Starting from Eq. (16), the steps are exactly as the previous case in Sec. A, except that in the vacuum region  $\rho(r) = 0$ . This leads to the homogeneous (i.e., source-free) wave equation that governs the scalar electric potential

$$\frac{d^2 f_\phi(r)}{dr^2} + \frac{1}{r} \frac{df_\phi(r)}{dr} - \tau^2 f_\phi(r) = 0, \quad (44)$$

where

$$\tau^2 = k^2 - k_0^2. \quad (45)$$

The general solution of the differential equation in Eq. (44) is a linear combination of modified Bessel functions,

$$f_\phi(r) = b_1 I_0(\tau r) + b_2 K_0(\tau r), \quad (46)$$

where  $b_1$  and  $b_2$  are arbitrary constants,  $I_0$  is the modified Bessel function of the first kind and order zero, and  $K_0$  is the modified Bessel function of the second kind and order zero.

#### APPENDIX C

##### CHARACTERISTIC EQUATION DEFINITION AND MODE PROFILE

We show the steps we used to find solutions to the system of equations in  $\underline{\mathbf{M}}\mathbf{c} = \mathbf{0}$ , where  $\mathbf{c} = [c_1, c_2, c_3, c_4, c_5, c_6, c_7]^T$  and the matrix  $\underline{\mathbf{M}}$  is given in Eq. (26). Once we assume the stream parameters and the radii of the structure, the only unknowns we are left with are the 7 constants in  $\mathbf{c}$  and the wavenumber  $k$ . First, we assume that the potential function at the center of stream region 1 (given by Eq. (19)) is normalized such that  $f_{\phi,1}(r=0) = c_1 = 1$  V.

Then, for a given wavenumber  $k$ , one finds the rest of the constants of the system by solving the last six equations described in  $\underline{\mathbf{M}}\mathbf{c} = \mathbf{0}$ , which yields

$$\begin{bmatrix} c_2 \\ c_3 \\ c_4 \\ c_5 \\ c_6 \\ c_7 \end{bmatrix} = \begin{bmatrix} \tau K_0'(\tau R_{1,1}) & \tau I_0'(\tau R_{1,1}) & 0 & 0 & 0 & 0 & 0 \\ K_0(\tau R_{1,2}) & I_0(\tau R_{1,2}) & -J_0(T_2 R_{1,2}) & -Y_0(T_2 R_{1,2}) & 0 & 0 & 0 \\ \tau K_0'(\tau R_{1,2}) & \tau I_0'(\tau R_{1,2}) & -T_2 J_0'(T_2 R_{1,2}) & -T_2 Y_0'(T_2 R_{1,2}) & 0 & 0 & 0 \\ 0 & 0 & J_0(T_2 R_{0,2}) & Y_0(T_2 R_{0,2}) & -K_0(\tau R_{0,2}) & -I_0(\tau R_{0,2}) & 0 \\ 0 & 0 & T_2 J_0'(T_2 R_{0,2}) & T_2 Y_0'(T_2 R_{0,2}) & -\tau K_0'(\tau R_{0,2}) & -\tau I_0'(\tau R_{0,2}) & 0 \\ 0 & 0 & 0 & 0 & K_0(\tau R_t) & I_0(\tau R_t) & 0 \end{bmatrix}^{-1} \begin{bmatrix} T_1 J_0'(T_1 R_1) \\ 0 \\ 0 \\ 0 \\ 0 \\ 0 \\ 0 \end{bmatrix}. \quad (47)$$

Reaching this stage, we found the seven constants in  $\mathbf{c}$ , which satisfy six out of the seven boundary conditions. The next step is that we solve to find the last unknown  $k$  that will satisfy the first boundary condition as

$$C_e = J_0(T_1 R_1) - c_2 K_0(\tau R_1) - c_3 I_0(\tau R_1) = 0. \quad (48)$$

We find solutions of  $k$  by searching for complex wavenumbers that guarantee that Eq. (48) is satisfied, which implicitly guarantees that the remaining equations are also satisfied since  $c_2$  and  $c_3$  are found based on satisfying the rest of the boundary conditions. The modes' profile in Fig. 2(a) is found based the constants calculated from Eq. (47) with  $c_1 = 1$  V to have a normalized electric potential at the center of stream 1 as  $f_\phi(r=0) = 1$  V.

#### APPENDIX D

##### EFFECT OF SWAPPING STREAM VELOCITIES

We show in Fig. 8(a) the magnitude of the value of the characteristic equation in log scale for the same case with results shown in Fig. 2(a), except that the beam dc voltages of the two streams are swapped, i.e.,  $V_{0,1} = 6$  kV and  $V_{0,2} = 7$  kV instead of  $V_{0,1} = 7$  kV and  $V_{0,2} = 6$  kV. We label the

four modes in Fig. 8(a) that correspond to the dominant modes of the system. Compared to the previous case, we still see that the interaction between the two streams results in instability.

In Fig. 9, we show the four modes of the two-stream system when the dc current of stream 2 is swept similarly to case shown in Fig. 3, except that the beam dc voltages of the two streams are swapped, i.e., now  $V_{0,1} = 6$  kV and  $V_{0,2} = 7$  kV, instead of  $V_{0,1} = 7$  kV and  $V_{0,2} = 6$  kV as in Fig. 3. The figures show that there exist two transition points (bifurcations) close to  $I_{0,2} = 1$  mA and  $I_{0,2} = 54.7$  mA, between which, exponentially growing space-charge waves occur due to the two-stream instability effect. This is similar to the other case in Fig. 3, except that the transition points in Fig. 3 occurred at approximately  $I_{0,2} = 2$  mA and  $I_{0,2} = 62.2$  mA.

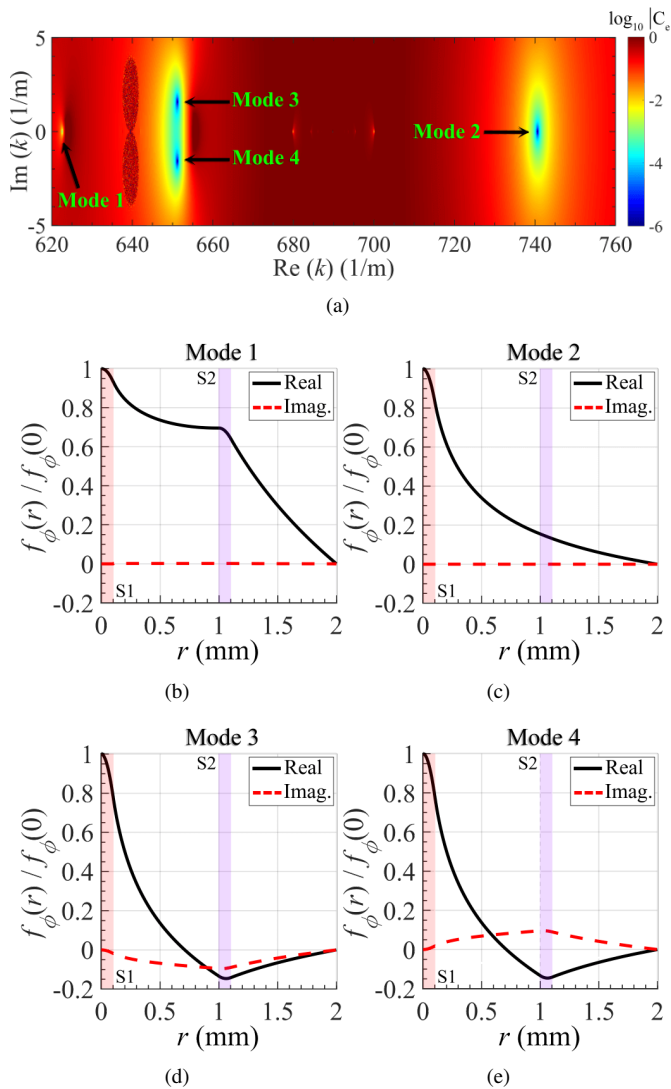


Fig. 8. (a) Values of  $C_e$  versus complex wavenumber  $k$ , evaluated at  $f = 5$  GHz, when the two streams dc voltages are  $V_{0,1} = 6$  kV and  $V_{0,2} = 7$  kV. (b)–(e) Normalized potential profiles corresponding to the four modes labeled in (a). These plots should be compared with those in Fig. 2, with the difference that the stream voltages have been inverted since in Fig. 2 we had  $V_{0,1} = 7$  kV and  $V_{0,2} = 6$  kV.

## REFERENCES

- [1] J. X. Qiu, B. Levush, J. Pasour, A. Katz, C. M. Armstrong, D. R. Whaley, J. Tucek, K. Kreischer, and D. Gallagher, “Vacuum tube amplifiers,” *IEEE Microwave Magazine*, vol. 10, no. 7, pp. 38–51, 2009.
- [2] J. H. Booske, R. J. Dobbs, C. D. Joye, C. L. Kory, G. R. Neil, G.-S. Park, J. Park, and R. J. Temkin, “Vacuum electronic high power terahertz sources,” *IEEE Transactions on Terahertz Science and Technology*, vol. 1, no. 1, pp. 54–75, 2011.
- [3] J. H. Booske, “Plasma physics and related challenges of millimeter-wave-to-terahertz and high power microwave generation,” *Physics of plasmas*, vol. 15, no. 5, p. 055502, 2008.
- [4] R. K. Parker, R. H. Abrams, B. G. Danly, and B. Levush, “Vacuum electronics,” *IEEE transactions on microwave theory and techniques*, vol. 50, no. 3, pp. 835–845, 2002.
- [5] A. Pobedonostev, E. Gelvich, M. Lopin, A. Alexeyenko, A. Negirev, and B. Sazonov, “Multiple-beam microwave tubes,” in *1993 IEEE MTT-S International Microwave Symposium Digest*, pp. 1131–1134, IEEE, 1993.
- [6] L. G. Y.-L. M. Sheng and L. Gang, “Multi-beam twt with active power combining,” *International journal of electronics*, vol. 84, no. 6, pp. 647–657, 1998.

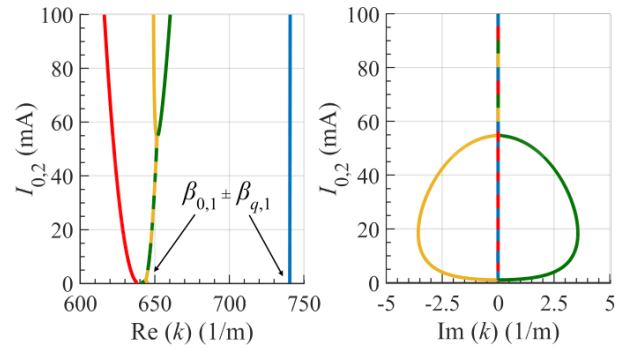


Fig. 9. Modal dispersion diagram of the complex-valued space-charge wavenumber as a function of stream 2 dc current. In this case we have  $V_{0,1} = 6$  kV and  $V_{0,2} = 7$  kV. These results should be compared with those in Fig. 3, with the difference that the stream voltages have been here inverted since in Fig. 3 we had  $V_{0,1} = 7$  kV and  $V_{0,2} = 6$  kV.

- [7] J. Pierce, “Double-stream amplifiers,” *Proceedings of the IRE*, vol. 37, no. 9, pp. 980–985, 1949.
- [8] D. Swift-Hook, “Validity of the theory of double stream amplification,” *Physical Review*, vol. 118, no. 1, p. 1, 1960.
- [9] G. Dohler, D. Gagne, and D. Zavadil, “Beam-beam interactions in concentric-beam dual-mode twt’s,” in *1980 International Electron Devices Meeting*, pp. 169–172, IEEE, 1980.
- [10] C. Chen, “Efficiency scaling law for the two-stream amplifier,” *Physics of Plasmas*, vol. 3, no. 8, pp. 3107–3110, 1996.
- [11] G. S. Nusinovich, S. J. Cooke, M. Botton, and B. Levush, “Wave coupling in sheet-and multiple-beam traveling-wave tubes,” *Physics of Plasmas*, vol. 16, no. 6, p. 063102, 2009.
- [12] D. A. Zavadil, “Dual beam dual mode twt,” in *1974 International Electron Devices Meeting (IEDM)*, pp. 209–211, IEEE, 1974.
- [13] A. Hollenberg, “Experimental observation of amplification by interaction between two electron streams,” *Bell System Technical Journal*, vol. 28, no. 1, pp. 52–58, 1949.
- [14] D. Neben, K. Bishofberger, V. Pavlenko, and N. Yampolsky, “A co-axial electron gun to generate millimeter-wave rf using the two-stream instability,” *Review of Scientific Instruments*, vol. 92, no. 5, p. 053301, 2021.
- [15] L. S. Nergaard, “Analysis of a simple model of a two-beam growing-wave tube,” *RCA Review*, vol. 9, no. 585, pp. 19–8, 1948.
- [16] A. V. Haeff, “The electron-wave tube—a novel method of generation and amplification of microwave energy,” *Proceedings of the IRE*, vol. 37, no. 1, pp. 4–10, 1949.
- [17] J. M. Butler and C. Wharton, “Twin traveling-wave tube amplifiers driven by a relativistic backward-wave oscillator,” *IEEE transactions on plasma science*, vol. 24, no. 3, pp. 884–894, 1996.
- [18] B. E. Carlsten, K. A. Bishofberger, and R. J. Faehl, “Compact two-stream generator of millimeter- and submillimeter-wave radiation,” *Physics of Plasmas*, vol. 15, no. 7, p. 073101, 2008.
- [19] K. Islam and E. Schamiloglu, “Multiple electron beam generation with different energies and comparable currents from a single cathode potential for high power traveling wave tubes (twts),” *Journal of Applied Physics*, vol. 131, no. 4, p. 044901, 2022.
- [20] K. N. Islam, L. D. Ludeking, A. D. Andreev, S. Portillo, A. M. N. Elfrgani, and E. Schamiloglu, “Modeling and simulation of relativistic multiple electron beam generation with different energies from a single-cathode potential for high-power microwave sources,” *IEEE Transactions on Electron Devices*, vol. 69, no. 3, pp. 1380–1388, 2022.
- [21] A. Figotin, *An Analytic Theory of Multi-stream Electron Beams in Traveling Wave Tubes*. World Scientific, 2020.
- [22] K. Evans, *Instability of the Two-Stream Electron-Beam System*. PhD thesis, University of California, Irvine, 2019.
- [23] A. F. Abdelshafy, M. A. Othman, F. Yazdi, M. Veysi, A. Figotin, and F. Capolino, “Electron-beam-driven devices with synchronous multiple degenerate eigenmodes,” *IEEE Transactions on Plasma Science*, vol. 46, no. 8, pp. 3126–3138, 2018.
- [24] A. Figotin and G. Reyes, “Multi-transmission-line-beam interactive system,” *Journal of Mathematical Physics*, vol. 54, no. 11, p. 111901, 2013.
- [25] A. Figotin, “Exceptional points of degeneracy in traveling wave tubes,” *Journal of Mathematical Physics*, vol. 62, no. 8, p. 082701, 2021.

- [26] M. A. Othman, M. Veysi, A. Figotin, and F. Capolino, "Low starting electron beam current in degenerate band edge oscillators," *IEEE Transactions on Plasma Science*, vol. 44, no. 6, pp. 918–929, 2016.
- [27] K. Rouhi, R. Marosi, T. Mealy, A. F. Abdelshafy, A. Figotin, and F. Capolino, "Exceptional degeneracies in traveling wave tubes with dispersive slow-wave structure including space-charge effect," *Applied Physics Letters*, vol. 118, no. 26, p. 263506, 2021.
- [28] F. Yazdi, M. A. Othman, M. Veysi, A. Figotin, and F. Capolino, "A new amplification regime for traveling wave tubes with third-order modal degeneracy," *IEEE Transactions on Plasma Science*, vol. 46, no. 1, pp. 43–56, 2017.
- [29] M. Boyd, R. Dehn, J. Hickey, and T. Mihran, "The multiple-beam klystron," *IRE Transactions on Electron Devices*, vol. 9, no. 3, pp. 247–252, 1962.
- [30] W. Pohl, "The design and demonstration of a wide-band multiple-beam traveling-wave klystron," *IEEE Transactions on Electron Devices*, vol. 12, no. 6, pp. 351–368, 1965.
- [31] Y. Ding, B. Shen, S. Shi, and J. Cao, "S-band multibeam klystron with bandwidth of 10%," *IEEE transactions on electron devices*, vol. 52, no. 5, pp. 889–894, 2005.
- [32] S. Yan, W. Su, Y. Wang, and A. Xu, "Design and theoretical analysis of multibeam folded waveguide traveling-wave tube for subterahertz radiation," *IEEE Transactions on Plasma Science*, vol. 43, no. 1, pp. 414–421, 2014.
- [33] S.-m. Yan, W. Su, and G.-l. Zhang, "Design and fabrication of a sub-millimeter multi-beam folded waveguide structure," *Optoelectronics Letters*, vol. 13, no. 1, pp. 33–37, 2017.
- [34] W. Liu, K. Li, P. Gao, C. Zhao, X. Guo, and Z. Zhang, "Nonlinear theory for beam-wave interactions of two electron beams with higher order te20 mode in serpentine waveguide traveling wave amplifier," *Physics of Plasmas*, vol. 25, no. 12, p. 123106, 2018.
- [35] N. Shi, H. Wang, D. Xu, Z. Wang, Z. Lu, H. Gong, D. Liu, Z. Duan, Y. Wei, and Y. Gong, "Study of 220 ghz dual-beam overmoded photonic crystal-loaded folded waveguide twt," *IEEE Transactions on Plasma Science*, vol. 47, no. 6, pp. 2971–2978, 2019.
- [36] Y. Yang and W. Ding, "A two-stream gyrotron traveling wave tube amplifier," *Physics of Plasmas*, vol. 6, no. 11, pp. 4328–4332, 1999.
- [37] Y.-M. Shin, L. R. Barnett, and N. C. Luhmann Jr, "Strongly confined plasmonic wave propagation through an ultrawideband staggered double grating waveguide," *Applied Physics Letters*, vol. 93, no. 22, p. 221504, 2008.
- [38] A. Gee and Y.-M. Shin, "Gain analysis of higher-order-mode amplification in a dielectric-implanted multi-beam traveling wave structure," *Physics of Plasmas*, vol. 20, no. 7, p. 073106, 2013.
- [39] J. Yang, K. Cai, G. Deng, Z. Yin, J. Ruan, F. Cai, and Y. Fang, "A staggered double-vane slow-wave structure with double sheet electron beams for 340 ghz traveling wave tube," *Journal of Electromagnetic Waves and Applications*, vol. 33, no. 12, pp. 1632–1643, 2019.
- [40] W. Shao, D. Xu, Z. Wang, H. Gong, Z. Lu, Z. Duan, Y. Wei, Y. Gong, and S. Aditya, "Stacked dual beam electron optical system for thz integrated wideband traveling wave tube," *Physics of Plasmas*, vol. 26, no. 6, p. 063106, 2019.
- [41] Z. Lu, K. Ding, R. Wen, W. Ge, M. Zhu, Z. Wang, H. Gong, and Y. Gong, "Novel double tunnel staggered grating slow wave structure for 0.2 thz traveling wave tube," *IEEE Electron Device Letters*, vol. 41, no. 2, pp. 284–287, 2020.
- [42] Z. Lu, M. Zhu, K. Ding, R. Wen, W. Ge, Z. Wang, T. Tang, H. Gong, and Y. Gong, "Investigation of double tunnel sine waveguide slow-wave structure for terahertz dual-beam twt," *IEEE Transactions on Electron Devices*, vol. 67, no. 5, pp. 2176–2181, 2020.
- [43] J. Luo, J. Xu, P. Yin, R. Yang, L. Yue, Z. Wang, L. Xu, J. Feng, W. Liu, and Y. Wei, "A 340 ghz high-power multi-beam overmoded flat-roofed sine waveguide traveling wave tube," *Electronics*, vol. 10, no. 23, p. 3018, 2021.
- [44] H. Wang, Z. Wang, X. Li, T. He, D. Xu, H. Gong, T. Tang, Z. Duan, Y. Wei, and Y. Gong, "Study of a miniaturized dual-beam twt with planar dielectric-rods-support uniform metallic meander line," *physics of plasmas*, vol. 25, no. 6, p. 063113, 2018.
- [45] G. V. Torgashov, R. A. Torgashov, V. N. Titov, A. G. Rozhnev, and N. M. Ryskin, "Meander-line slow-wave structure for high-power millimeter-band traveling-wave tubes with multiple sheet electron beam," *IEEE Electron Device Letters*, vol. 40, no. 12, pp. 1980–1983, 2019.
- [46] Z. Wen, J. Luo, Y. Li, W. Guo, M. Zhu, and F. Zhu, "A concentric arc meander line sws for low voltage, high efficiency, and wide bandwidth v-band twt with dual sheet beam," *IEEE Transactions on Plasma Science*, vol. 49, no. 6, pp. 1842–1847, 2021.
- [47] J. Liao, G. Shu, J. He, J. Ren, J. Lin, J. Deng, Z. Chang, B. Xu, C. Ruan, and W. He, "A terahertz band te20 mode input/output coupling structure for dual-sheet-beam traveling-wave tubes," *IEEE Transactions on Plasma Science*, vol. 50, no. 5, pp. 1360–1368, 2022.
- [48] R. A. Torgashov, A. G. Rozhnev, and N. M. Ryskin, "Design study on a multiple-tunnel meander-line slow-wave structure for a high-power v-band traveling-wave tube," *IEEE Transactions on Electron Devices*, vol. 69, no. 3, pp. 1396–1401, 2022.
- [49] S. Ramo, "Space charge and field waves in an electron beam," *Physical Review*, vol. 56, no. 3, p. 276, 1939.
- [50] G. Branch and T. Mihran, "Plasma frequency reduction factors in electron beams," *IRE Transactions on Electron Devices*, vol. 2, no. 2, pp. 3–11, 1955.
- [51] J. Pierce, "Waves in electron streams and circuits," *Bell System Technical Journal*, vol. 30, no. 3, pp. 626–651, 1951.
- [52] J. Pierce, "Theory of the beam-type traveling-wave tube," *Proceedings of the IRE*, vol. 35, no. 2, pp. 111–123, 1947.
- [53] L. J. Chu and J. D. Jackson, "Field theory of traveling-wave tubes," *Proceedings of the IRE*, vol. 36, no. 7, pp. 853–863, 1948.
- [54] C. A. Balanis, "Auxiliary vector potentials, construction of solutions, and radiation and scattering equations," in *Advanced engineering electromagnetics*, ch. 6, p. 262, John Wiley & Sons, 2012.
- [55] A. K. Cline, C. B. Moler, G. W. Stewart, and J. H. Wilkinson, "An estimate for the condition number of a matrix," *SIAM Journal on Numerical Analysis*, vol. 16, no. 2, pp. 368–375, 1979.
- [56] J. R. Pierce and W. B. Hebenstreit, "A new type of high-frequency amplifier," *The Bell System Technical Journal*, vol. 28, no. 1, pp. 33–51, 1949.
- [57] G. W. Hanson, A. B. Yakovlev, M. A. Othman, and F. Capolino, "Exceptional points of degeneracy and branch points for coupled transmission lines—Linear-algebra and bifurcation theory perspectives," *IEEE Transactions on Antennas and Propagation*, vol. 67, no. 2, pp. 1025–1034, 2019.
- [58] P. M. Phillips, E. Zaidman, H. Freund, A. K. Ganguly, and N. R. Vanderplaats, "Review of two-stream amplifier performance," *IEEE transactions on electron devices*, vol. 37, no. 3, pp. 870–877, 1990.
- [59] V. A. Tamma and F. Capolino, "Extension of the pierce model to multiple transmission lines interacting with an electron beam," *IEEE Transactions on Plasma Science*, vol. 42, no. 4, pp. 899–910, 2014.
- [60] N. W. McLachlan, "Bessel functions for engineers," *University of Illinois, Oxford University Press, London, England*, 1961.